Attitude Stabilization of Flexible Spacecraft During Stationkeeping Maneuvers

Bong Wie* and Carl T. Plescia†
Ford Aerospace & Communications Corporation, Palo Alto, California

This paper presents the analysis and design of a reaction jet attitude control system for a spacecraft having large flexible solar arrays. During translational thrusting maneuvers, the solar array flexibility interacts strongly with the pulse-width and pulse-frequency modulator. A simple transfer function model of flexible spacecraft is used for the preliminary control design. The static and dynamic characteristics of the modulator are discussed in detail. Nonlinear stability analysis is performed using the describing function of the modulator. Relative stability margin, with respect to the limit cycle condition of a structural mode, is used as a measure of the nonlinear control system robustness. The performance and stability margin predicted by classical single-axis design are verified from the three-axis nonlinear digital simulations.

Introduction

MANY three-axis staiblized geosynchronous communciations satellites (CTS, INTELSAT V, SATCOM, TDRS, INSAT, and ARABSAT) have large solar panel arrays with significant structural flexibility. The structural mode interaction with attitude control system has been one of the primary concerns for the design of three-axis stabilizied spacecraft.[1-3] Severe sructural/control lop interactions have also been reported for dual-spin spacecraft such as OSO-8[4] and Galileo.[5] Recently considerable attention has been directed toward the dynamic analysis and control system design for large flexible space structures.[6-11]

This paper presents the analysis and design of a microprocessor-based reaction jet attitude control system for a flexible spacecraft during translational thrusting maneuvers. Figure 1 shows a three-axis stabilized geosynchronous communications satellite having large flexible solar arrays erected north and south from a box-shaped central body. The antenna reflectors are rigidly mounted (after deployment) to the central body. The x axis is nominally in the flight direction, the y axis is normal to the orbit plane, and the z axis is directed to the Earth. The spacecraft control axes are assumed coincident with the principal axes of the spacecraft.

The roll/yaw coupling due to the pitch bias momentum is the unique feature of bias-momentum three-axis stabilization to control yaw error passively with a direct yaw measurement during on-orbit normal mode operations. The solar array flxibility does not interact seriously with the normal mode controller using skewed bias momentum wheels.[12] All of the structural modes are gain-stabilized by steep rolloff of the normal controller at a frequency well below the first sructural mode.

However, high loop gain is needed to maintain accurate body pointing in the presence of large disturbance torques during translational thrusting maneuvers. The solar array flexibility interacts strongly with the pulse-width and pulse-frequency (PWPF) modulator of the stationkeeping attitude control loop. Structural mode instability in the high-gain nonlinear control system often manifests as a limit cycles.[13-15] The relative stability margin with respect to the limit cycle condition of a structural mode may be used as some measure of the nonlinear control system robustness. The control loop nonlinearities include: the digital sensor quantization and saturation, the loop deadband, and the PWPF modulator. The structural mode instability is also caused by the Earth sensor sample and zero-order-hold delay of 0.25 s and by the microprocessor sampling (64 ms) and pure computational delay of 48 ms.

To reduce the structural mode interactions, a lower rigid-body bandwidth is desirable by applying a torque bias to the PWPF modulator. A closed-loop torque bias scheme can be implemented by the classical integral control or by the disturbance estimation using Kalman filter.[16] However, an open-loop torque prebias by ground command was selected for the spacecraft in this paper. The implementation of the torque prebias scheme is the subject of a Ford Aerospace and Communications Corporation patent application.[17] While the open-loop torque prebias requires an extensive on-orbit calibration of thrusters, it has a distinct advantage of the feed-forward open-loop control. Despite the lower rigid-body bandwidth, the structural mode interactions with the control loop nonlinearities need to be considered in the control system design.

Performance Requirements and Control System Descriptions

To maintain the spacecraft position in geosynchronous orbit to within ± 0.1 deg, the spacecraft shown in Fig. 1, requires about six north/south stationkeeping maneuvers per year, each with a duration of maximum 2 min. East/west corrections are made at approximately 12-day intervals with duration of only a few seconds. The reaction jet attitude control system (22-N thrusters) must counteract disturbance torques due to thruster misalignment, plume impingement, and mismatch between pairs of thrusters used to impart velocity changes during these maneuvers. Attitude pointing requirements are to maintain spacecraft short-term attitude errors within ± 0.06 deg in roll/pitch and ± 0.1 deg in yaw. The control loop should not have structural mode limit cycle oscillation in the presence of $\pm 20\%$ control torque-to-inertia ratio variation and $\pm 20\%$ structural mode uncertainty throughout 7-yr mission lifetime. It is assumed that 75% of

Submitted June 16, 1983; presented as Paper 83-2226 at the AIAA Guidance and Control Conference, Gatlinburg, Tenn., Aug. 15-17, 1983; revision received Nov. 15, 1983.

*Engineering Specialist, Systems Analysis Department. Member AIAA.

†Sr. Engineering Specialist, Systems Analysis Department. Member AIAA.

the actual disturbance torques (±2.0 Nm max) can be biased leaving a residual uncertainty of ±0.5 Nm max to be controlled by the feedback control system. The stationkeeping attitude controller also provides three-axis stabilization during initial station acquisition, momentum wheel spin-up, and station relocations.

Figure 2 shows a block diagram of the stationkeeping attitude control sytem. The Earth sensor provides roll/pitch attitude references, while the rate integrating gyros (RIG's) provide yaw attitude reference and three-axis body rates during the stationkeeping mode operations. The control logic for direct attitude error/rate feedback, structural filtering, and PWPF modulation is implemented in the microprocessor with a 64-ms sampling period. There is no cross-axis feedback control. The sun sensor in the yaw channel provides yaw attitude reference in case of RIG failure. The rate loop has a high-pass filter to wash out any residual drift rate bias (up to 1 deg/h) of RIG.

The signal after structural filtering (optional) is then passed through the loop deadband, the loop gain, and the PWPF modulator, which in turn activates the thruster valves. The PWPF modulator causes a pulse command on the average by adjusting the pulse width and pulse frequency. Since the roll thrusters are utilized in pairs for N/S thrusting maneuvers, they will be off-modulated to be used for roll attitude control while pitch and yaw thrusters are on-modulated. Similarly, when the pitch or yaw thrusters are used for E/W maneuvers, they provide the spacecraft velocity changes and are off-modulated for attitude control.

Flexible Spacecraft Models

The hybrid-coordinate model[18] was used for the control analysis, design, and digital simulations. A finite element analysis using NASTRAN was performed to obtain the cantilever frequencies and rigid-elastic coupling matrix of the hybrid-coordinate model. A single solar array flexibility model referenced to the spacecraft center of mass is given in Table 1. Orbit time of 6 a.m. yields out-of-plane bending modes in yaw axis and in-plane bending modes in roll axis. The low-frequency characteristic of the first in-plane mode is caused by array yoke deformation. The antenna reflector flexibility is neglected because of its high frequency and smaller rigid-elatic coupling scalar.

Table 1 Single solar array flexibility model at 6 a.m.

Mode description[a]	Cantilever frequency, rad/s	Coupling matrix $(kg \cdot m^2)^{0.5}$		
		Roll	Pitch	Yaw
OP-1	0.885	0	0	35.372
OP-2	6.852	0	0	4.772
OP-3	16.658	0	0	2.347
OP-4	33.326	0	0	0.548
T-1	5.534	0	2.532	0
T-2	17.668	0	0.864	0
T-3	33.805	0	0.381	0
IP-1	1.112	35.865	0	0
IP-2	36.362	2.768	0	0

[a] OP = out-of-plane, T = torsion, IP = in-plane.

Table 2 Spacecraft nominal parameters (6 a.m.)

Parameter descriptions	Roll	Pitch	Yaw
Spacecraft inertia, $kg \cdot m^2$	3026	440	3164
Control torque, N·m	10	10	10
Residual disturbance, N·m	0.5	0.5	0.5
Pointing requirement, deg	0.06	0.06	0.1
Structural mode zero, rad/s	1.11	5.53	0.88
Structural mode pole, rad/s	2.87	5.61	1.93

The linearized equations of motion are
Rigid body

$$I\ddot{\theta}+H\dot{\theta}+D^T\ddot{q}=T_c+T_d \tag{1a}$$

Solar arrays

$$\ddot{q}+\sigma^2 q+D\ddot{\theta}=0 \tag{1b}$$

where I is the entire spacecraft inertia matrix, H is the momentum coupling matrix, D is the rigid-elastic coupling matrix of two arrays (function of solar array slew angle), θ is the attitude angle vector, q is the cantilever modal coordinate vector, σ is the cantilever modal frequency vector, T_c is the control torque vector, and T_d is the disturbance torque vector. A passive modal damping ratio of 0.002-0.005 is usually added to Eq. (1b). The passive structural damping is needed to gain-stabilize the higher structural modes. Table 2 summarizes the nominal spacecraft parameters.

Since the nutation frequency, $h/\sqrt{I_x I_z}=0.02$ rad/s, is well below the stationkeeping attitude controller bandwidth of about 1.0 rad/s, the nutation mode is approximated as a double pole at the origin. A single-axis transfer function from control torque to attitude angle output can then be represented as

$$G(s)=\frac{1}{Is^2}\prod_{i=1}^{N}\frac{(s^2/z_i^2+1)}{(s^2/p_i^2+1)} \tag{2}$$

where s is the Laplace transform variable, I is the entire spacecraft inertia, z_i is the ith zero, p_i is the ith pole, and N is the total number of flexible modes. A passive structural damping ratio of 0.002-0.005 can be added directly to the numerator and denominator of Eq. (2) for the realistic controller design.

As shown by Martin and Bryson[9] the transfer function given by Eq. (2) has alternating poles and zeros along the imaginary axis because the actuator and sensor are "colocated" at the rigid central body. When the actuator and sensor are colocated, the rigid-body mode and all the structural modes are "stably" interacting with each other. Despite the colocated actuator and sensor, the control design requires great care because of the structural mode interations with the control loop nonlinearities. The cross-axis transfer function from yaw (roll) torque to roll (yaw) output has, however, nonalternating poles and zeros, which results in "unstable" interactions of structural modes with the rigid-body mode.[12]

During the N/S maneuvers the south array is oriented to minimize the thermal effects of thruster firings on the solar cells. Thus the out-of-plane bending is coupled to the spacecraft yaw motion. Such south array orientation also reduces the effects of plume impingement torques on the

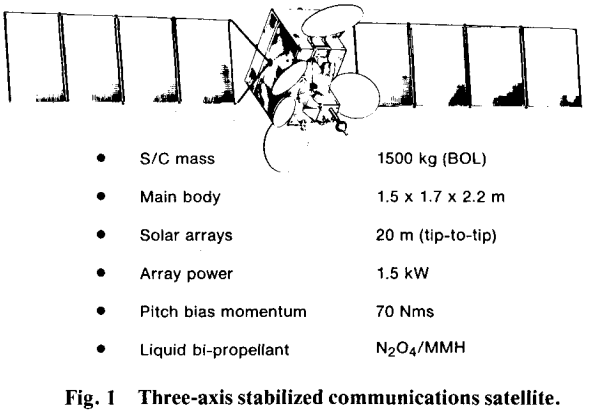

Fig. 1 Three-axis stabilized communications satellite.

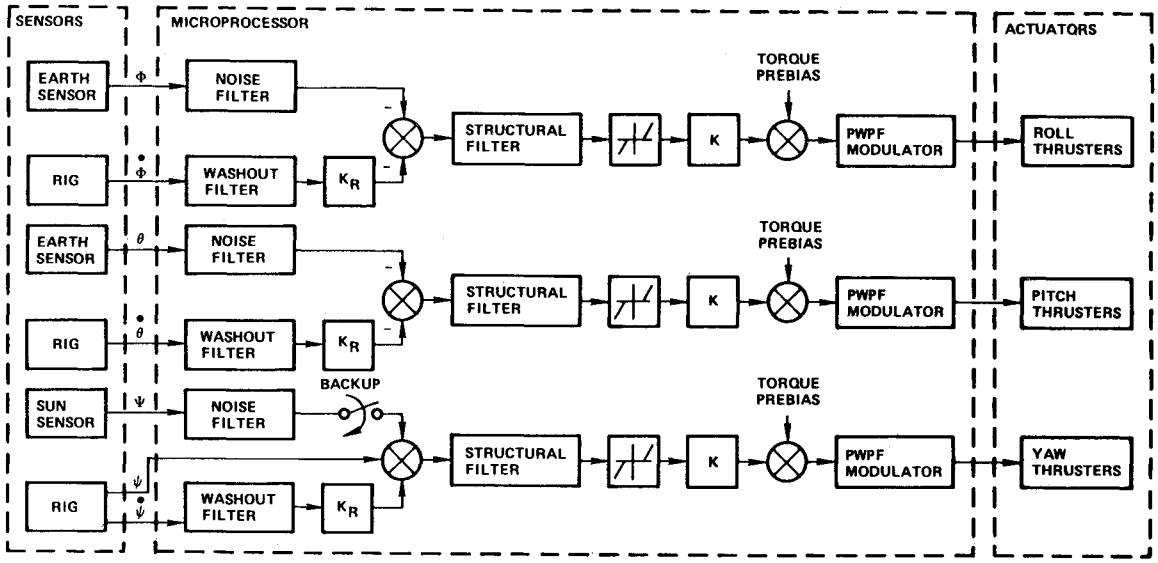

Fig. 2 Control system block diagram.

spacecraft attitude control. Since there are no thrusters on the spacecraft north face, the north array is always pointing to the sun.

During the N/S or E/W maneuvers at 6 a.m., both arrays are pointing to the sun. A single-axis transfer function with a single dominant structural mode can then be simply obtained as

$$G(s) = \frac{s^2 + \sigma^2}{Is^2\,[\,(1 - 2\delta^2/I)s^2 + \sigma^2\,]} \tag{3}$$

where σ and δ are the cantilever frequency and the rigid-elastic coupling scalar of the dominant mode of a single array in Table 1, respectively. The factor of 2 in the denominator of Eq. (3) comes from the symmetry of two arrays. For the N/S maneuvers at noon where both arrays are perpendicular to each other, a single-axis transfer function with two dominant structual modes can also be obtained as

$$G(s) = (s^2 + \sigma_1^2)\,(s^2 + \sigma_2^2) \Big/ \left\{ Is^2 \left[\left(1 - \frac{\delta_1^2 + \delta_2^2}{I} \right) s^4 + \left(\sigma_1^2 + \sigma_2^2 - \frac{\delta_1^2 \sigma_2^2}{I} - \frac{\delta_2^2 \sigma_1^2}{I} \right) s^2 + \sigma_1^2 \sigma_2^2 \right] \right\} \tag{4}$$

where (σ_1, δ_1) and (σ_2, δ_2) correspond to the dominant out-of-plane and in-plane bending modes of a single array in Table 1, respectively.

Using Eq. (3), the dominant structural mode poles at 6 a.m. can be found as 2.87 rad/s in roll, 5.61 rad/s in pitch, and 1.93 rad/s in yaw. These approximate values agree closely with the values obtained by a computer program for the model given by Eqs. (1). The effect of the pitch bias momentum (70 Nms) on the free-free structural modes is negligible here. The effect of the higher fequency cantilever modes with a smaller coupling scalar on the first dominant free-free structural mode is also negligible. Equation (3) or (4) is the simple transfer function model of flexible spacecraft for the preliminary control analysis and design.

PWPF Modulator Analysis

The PWPF modulator produces a pulse command sequence to the thruster valves by adjusting the pulse width and pulse frequency. In the linear range, the average torque produced equals the demanded torque input. Several different on-off

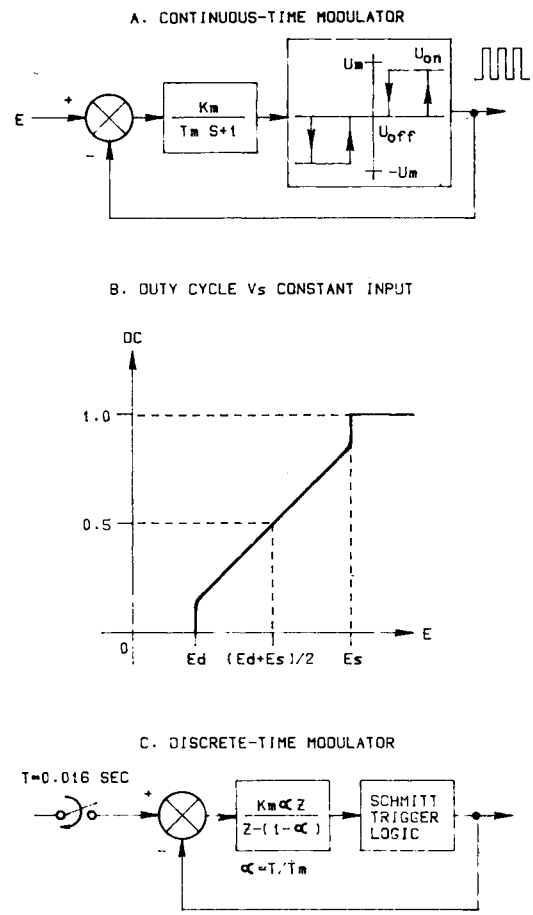

Fig. 3 PWPF modulator.

modulation techniques[19] have been used for the reaction jet control systems. The pulse width and pulse frequency of such modulations are usually fast compared to the spacecraft rigid-body dynamics, and the static characteristics of the modulator were good enough, in the past, for rigid spacecraft attitude controls. Recently, dynamic characteristics of the modulator have been investigated in Refs. 13-15 for flexible spacecraft attitude controls. Only the PWPF modulator shown in Fig. 3 will be discussed in this paper. This PWPF modulator is, in

fact, identical to the derived-rate modulator with an additional filter (same as the filter in the feedback loop) at the input.

With a constant input, the PWPF modulator drives the thruster valve with an on-off pulse sequence having a nearly linear duty cycle with input amplitude. The duty cycle or modulation factor is defined as the average output of the modulator. The static characteristics of the continuous-time modulator for a constant input E are as follows:

Minimum pulse width

$$\Delta = -T_m \ell n [1 - h/K_m U_m] \cong T_m h/K_m U_m \tag{5a}$$

Duty cycle

$$\mathrm{DC} = \left[\frac{[\ell n (1 + a/(1-x))]}{1 + \ell n (1 + a/x)} \right]^{-1} \tag{5b}$$

Internal deadband

$$E_d = U_{\mathrm{on}}/K_m \tag{5c}$$

Saturation level

$$E_s = U_m + U_{\mathrm{off}}/K_m \tag{5d}$$

where

$$h = u_{\mathrm{on}} - U_{\mathrm{off}} = \text{hysteresis width}$$

$$a = h/K_m (E_s - E_d) = \text{normalized hysteresis width}$$

$$x = (E - E_d)/(E_s - E_d) = \text{normalized input}$$

The U_{on}, U_{off}, U_m, K_m, and T_m are design parameters on the modulator shown in Fig. 3a. A typical plot of the duty cycle which is nearly linear over the range above deadband and below saturation is shown in Fig. 3b. A linearized duty cycle can be obtained by Taylor series approximation of Eq. (5b) about $x = 0.5$ (Ref. 19).

$$\mathrm{DC} = 0.5 + [2a/(1+2a)\ell n(1+2a)](x - 0.5) \tag{6}$$

which is invalid near $x = 0$ and 1.0. From Eq. (6), an effective deadband of about $E_d/2$ for $E_s = 1.0$ can be obtained.

A discrete-time PWPF modulator for microprocessor implementation is shown in Fig. 3c. The modulator gets an input signal every 64 ms and causes pulse command updates every 16 ms with pulse-width quantization of 16 ms. The digital implementation of a PWPF modulation is the subject of a Ford Aerospace and Communications Corporation patent application.[20] Equation (5a) derived for a continuous-time modulator becomes invalid for a discrete-time modulator. An inequality relation for the discrete-time PWPF modulator of 16-ms minimum pulse width can be found as

$$h < K_m U_m T/T_m < 2U_{\mathrm{on}} \tag{7}$$

where T is the modulator sampling period of 16 ms. The inequality of Eq. (7) at the right-hand side prevents a limit cycling of the modulator itself due to a large step in numerical integration.

The static characteristics of the modulator may be sufficient for rigid spacecraft attitude controls, but the dynamic characteristics need to be investigated for flexible spacecraft attitude controls. The dynamic characteristics can be simply analyzed using describing functions. The single-input describing function (SIDF) of a continuous-time modulator depends on the amplitude and frequency of input signal. If it can be assumed that there exists a minimum amplitude input A_m required to produce a single pulse width, then the gain and phase of the SIDF boundary, $N(A_m, j\omega)$, can be determined analytically as

$$\text{Gain (dB)} = 20 \log (B/A_m) \tag{8a}$$

$$\text{Phase (deg)} = -57.3 \tan^{-1} (T_m \omega) \tag{8b}$$

where

$$A_m = [U_{\mathrm{on}} - h/(1 + \exp(\Delta/T_m\omega))][(T_m\omega)^2 + 1]^{0.5}/K_m$$

$$B = [B_1^2 + B_3^2]^{0.5}$$

$$B_1 = (4/\pi) U_m \sin(\Delta\omega/2)$$

$$B_3 = (4/3\pi) U_m \sin(3\Delta\omega/2)$$

ω = input frequency (rad/s)

Δ = minimum pulse width (s)

The so-called corrected-conventional describing function is used where the rms value of the fundamental and third harmonic, and only the phase of the fundamental are taken. Equations (8) can be assumed to be valid for the discrete-time modulator because of a relatively fast sampling period of 16 ms compared to the frequency range below 10 rad/s.

The modulator provides an effective loop gain reduction at lower frequency and an additional phase lag at higher frequency. The phase lag of the modulator decreases as the time constant T_m decreases. However, a minimum value of T_m is about 0.1 s due to the microprocessor implementation with 16-ms sampling period. For a given minimum pulse width, the internal deadband increases as the T_m decreases. Thus, a tradeoff between the phase lag and the size of internal deadband is needed for the design of an optimal modulator.

Control Analysis and Design

The microcprocessor sampling period of 64 ms is relatively fast compared to the control bandwidth of about 0.5 rad/s and to the dominant flexible mode frequency of about 3.0 rad/s. This made it possible to use continuous-time design procedures for digital control design.[21] Classical design technicques such as a s-dominant root locus and a Bode plot were used. The pure time delay and the zero-order-hold delay are approximated as:

Pure time delay:

$$e^{-Ts} \cong \frac{T^2 s^2/8 - Ts/2 + 1}{T^2 s^2/8 + Ts/2 + 1}$$

Sample and zero-order-hold:

$$\frac{1 - e^{-Ts}}{Ts} \cong \frac{1}{T^2 s^2/12 + Ts/2 + 1}$$

For a relatively fast sampling rate, the sample and zero-order-hold delay can be approximated as $T/2$ s pure delay.

The s-domain design model for the roll axis is shown in Fig. 4. The combined effect of the microprocessor sampling (64 ms) and pure computational delay of 48 ms is approximated as a 80-ms pure time delay. The loop gain, K, determines the steady-state pointing accuracy for a constant disturbance torque during the maneuvers. The rate-to-position gain ratio, K_R, determines the closed-loop damping. The amplitude and rate of the rigid-body limit cycle are determined by the deadband and the modulator. The structural compensation filter provides additional gain and phase margins for the structural mode with respect to the limit cycle condition. The controller parameters including the structural filter are

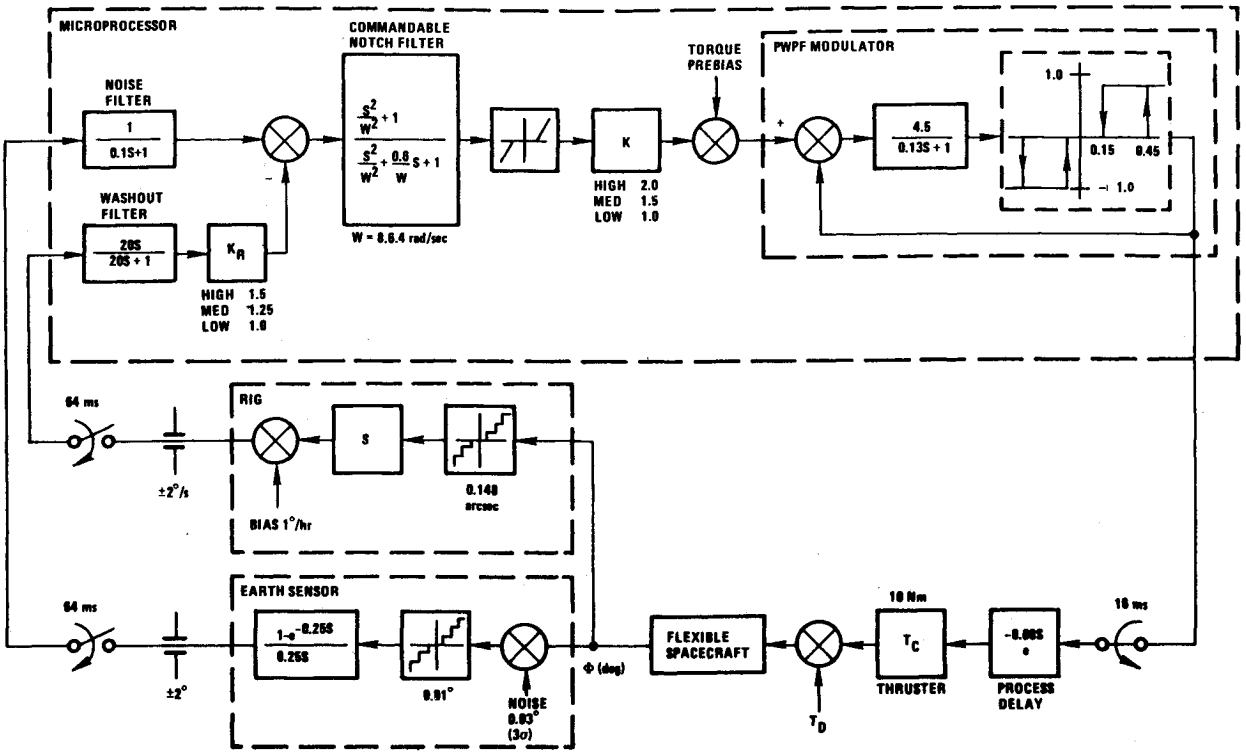

Fig. 4 Roll-axis control loop.

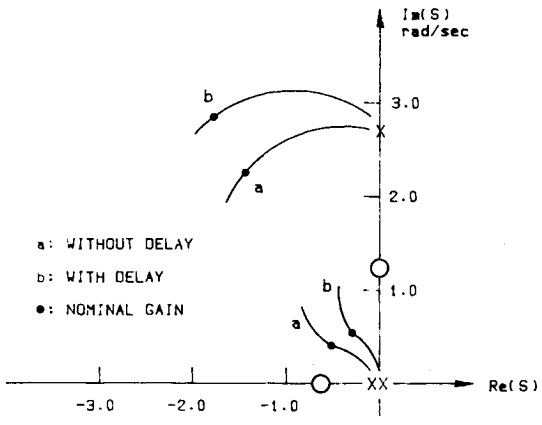

Fig. 5 Roll axis root locus vs overall loop gain ($K_R = 1.5$).

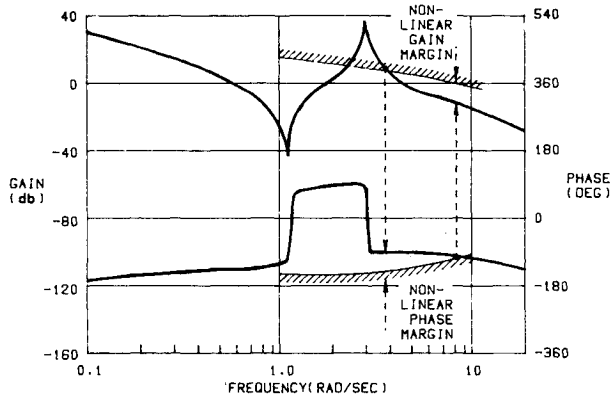

Fig. 6 Roll axis Bode plot ($K_R = 1.5$).

ground-commandable to cover the spacecraft parameter uncertainties throughout the 7-yr mission lifetime.

A second-order filter represented by

$$\frac{s^2/\omega_z^2 + 2\zeta_z s/\omega_z + 1}{s^2/\omega_p^2 + 2\zeta_p s/\omega_p + 1} \quad \text{or} \quad \frac{(T_1 s^2 + T_2 s + 1)}{(T_3 s^2 + T_4 s + 1)}$$

was discretized for microprocessor implementation. By different choices of the coefficients, several well-known frequency shaping filters can be obtained. For $\omega_z = \omega_p$ and $\zeta_z = 0.0$, we have a notch filter for gain-stabilization. The notch sharpness depends on the damping ratio of notch pole. Great care must be exercised in selecting the notch parameters because of its phase lag at low frequency and its sensitivity to structural mode uncertainty. For $\omega_z = \omega_p$ and $\zeta_p = 0.0$, we have a resonant filter to cancel the first structural mode zero if it is located inside the rigid-body control bandwidth. For $\omega_p > \omega_z$, we have a complex-lead or double-lead filter for phase-lead stabilization. The amount of phase lead depends primarily on the ω_p/ω_z ratio. But the ratio should not be too high because of the gain increase at higher frequencies. With $T_1 = 0.0$, we have a second-order lead compensation filter[9,22] for a rigid-body mode compensation in case of rate gyro failure.

The effective gain reduction of the deadband and PWPF modulator at the nominal operating point (0.5 Nm disturbance torque) was used for linear root-locus analysis. The sensor quantization and saturation are neglected for the preliminary linear analysis. Figure 5 is a typical root locus vs the effective loop gain without structural filter. The sensor/microprocessor delay effect can be seen from the figure. The linear design was then improved using a Bode plot with the describing function description of the modulator. The inverse of SIDF boundary of a typical PWPF modulator is shown on the Bode plot in Fig. 6. Consequently, the linear stability boundary of 0 dB and -180 deg lines on a Bode plot has been changed to the new nonlinear stability boundary. The relative stability margin with respect to the limit cycle condition of a structural mode was then defined as in Fig. 6. The linear loop transfer function includes the sensor/microprocessor delay. Such stability margin may be used as a measure of nonlinear control sytem robustness for a flexible spacecraft.

The rigid-body mode was phase-stabilized, i.e., closed-loop stable regardless of how high the loop gain is raised. The first dominant structural mode in each axis contains most of the eleastic vibration energy with low frequency close to the rigid-body control bandwidth. Thus gain-stabilization using passive filtering (multilag compensation) is not possible without a serious degradation of the rigid-body mode stability and performance. Consequently, phase-stabilization of such a dominant structural mode is unavoidable and accomplished by carefully considering the additional phase lag from the sensor/microprocessor delay and from the modulator.

From Fig. 6 it can be seen that the dominant structural mode has approximately a gain margin of 10 dB and phase margin of 45 deg with respect to the limit cycle condition. Such nonlinear stability margins are much less than the linear stability margins without the PWPF nonlinearity. Due to the loop time delay which produces large phase lag at a higher frequency without any gain attenuation, the dominant structural mode in each axis becomes more closed-loop stable as the modal frequency becomes lower. This property is not present in a flexible spacecraft without pure time delay in the control loop. The higher structural modes are gain-stabilized by the passive structural damping ratio of 0.002 and by the control loop attenuation at higher frequency.

The spacecraft with +50% structural frequency variation and with a nominal gain set has, obviously, less stability margin than the nominal spacecraft. To provide more stability margin for the structural mode, the rate-to-position gain ratio K_R is reduced with an increase only in the transient overshoot during maneuver startup. This property is somewhat unconventional for a flexible spacecraft with a linear control system. A slight reduction in the rigid-body performance could increase the stability of structural modes without necessity of a higher-order compensation. However, for the case with a strict pointing requirement, including the transient overshoot, the second-order structural filter can be used for the additional capability of preventing structural mode limit cycle by phase lead or gain attenuation near the limit cycle frequency. A closed-loop adaptive tuning of the structural filter and/or the gain, without involvement of the ground operator, may be desirable in some cases. However, practial implementation of the autonomous adaptive controller to the commercial communications satellite needs further investigation.

Digital Simulations

Three-axis nonlinear digital computer simulations have been performed to verify and improve the preliminary analytical design. The simulation results showed a reasonable agreement with the preliminary design based on the root locus and Bode plot. The computer program includes: 1) the hybrid-coordinate spacecraft model, 2) the same control software as implemented on the microprocessor, 3) digital sensor sampling, quantization, saturation, and noise effects, 4) thruster torques with cross-axis coupling and plume impingement, etc. It has been verified that the rate-to-position gain ratio K_R is a critical parameter for the overall stability and performance. Increasing the rate gain to achieve better damping ratios of 0.5-0.707 (optimal number in linear control analysis) for a rigid-body mode as well as for dominant flexible modes (in roll/yaw axis) turned out to be unacceptable in the presence of

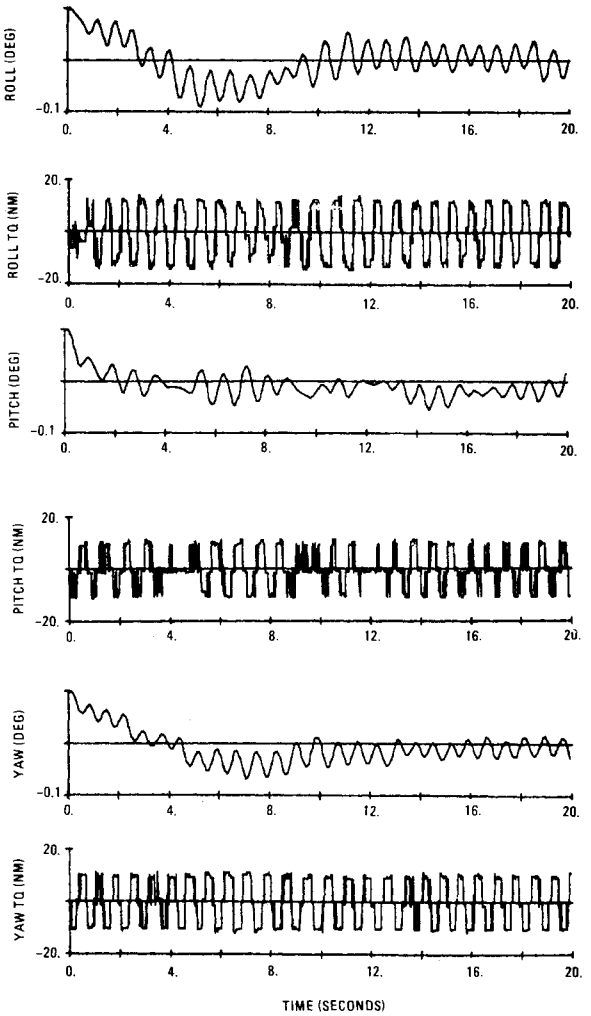

Fig. 7 Structural mode limit cycle oscillation.

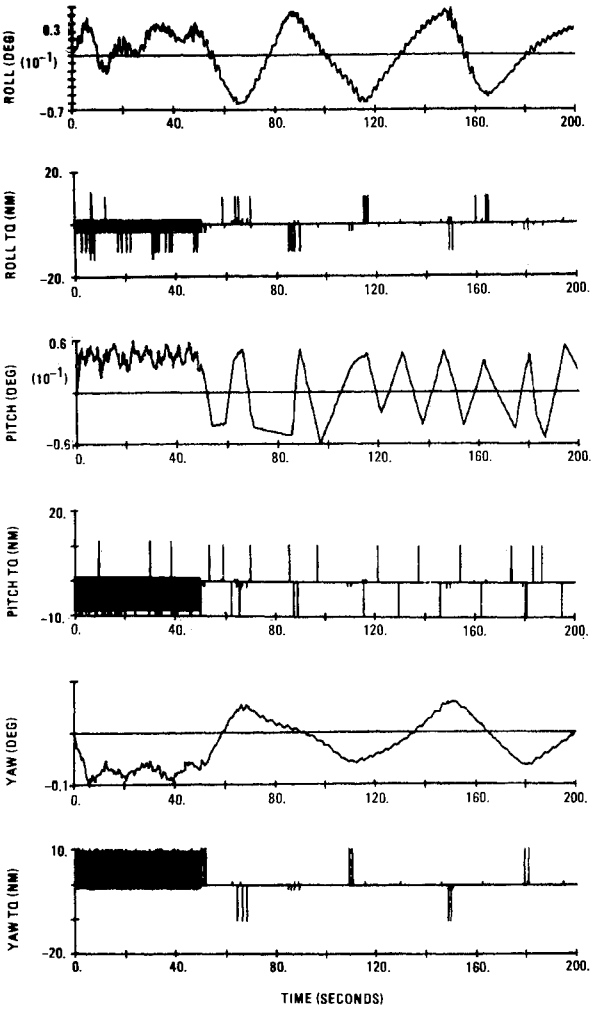

Fig. 8 Nominal responses for N/S maneuver.

the structural mode interactions with the PWPF modulator nonlinearity.

The existence of a structural mode limit cycle, predicted from describing function analysis, was verified from the digital simulations. Figure 7 shows a typical limit cycling of the structural modes in the roll/yaw axis. The limit cycle frequency is about 5 rad/s. Because of the three-axis couplings and sensor noise, the limit cycle is not as simple as predicted from the analysis. It was difficult to have a structural model limit cycle with a minimum pulse width. However, the describing function analysis on a Bode plot provided a simple way of designing the PWPF modulator for a flexible spacecraft. Figure 8 shows nominal responses for a N/S maneuver where roll thrusters are off-modulated while pitch/yaw thrusters are on-modulated. The maneuver duration was 50 s. The amplitude and rate of the rigid-body limit cycle after maneuver is acceptable for the transition mode operations.[12]

Conclusions

The analysis and design of a nonlinear attitude control system for a spacecraft having large flexible solar arrays was presented. A heuristic analytical design procedure based on the root locus and Bode plot was proved by digital simulations to be adequate for the design of a microcprocessor-based nonlinear control system. The describing function analysis of the modulator on a Bode plot provided a simple way of analyzing and designing a thruster-modulated attitude control system for a flexible spacecraft. The ground-commandability of the torque prebias, the variable gains, and the structural filters was a key factor for a successful design using the classical techniques. An autonomous spacecraft with a significant parameter uncertainty, however, may need advanced techniques such as on-orbit parameter identification and/or adaptive control.

References

[1]Hughes, P.C. and Garg, S.C., "Dynamics of Large Flexible Solar Arrays and Application to Spacecraft Attitude Control System Design," University of Toronto, Toronto, Canada, UTIAS Rept. 179, Feb. 1973.

[2]Gething, J.M. et al., "Effects of Flexibility on a Momentum-Stabilized Communication-Satellite Attitude Control System," *Proceedings of the IEEE,* Vol. 120, No. 5, May 1978, pp. 613-619.

[3]"Intelsat V Spacecraft Attitude Control Subsystem Analysis Rept.," Vol. II, Ford Aerospace, Palo Atlo, Calif., WDL-TR7518B, June 2, 1978.

[4]Yocum, J.F. and Slafer, L.I., "Control System Design in the Presence of Severe Structural Dynamics Interactions," *Journal of Guidance and Control,* Vol. 1, March-April 1978, pp. 109-116.

[5]Kopf, E.H., Brown, T.K., and Marsh, E.L., "Flexible Stator Control on the Galileo Spaceraft," Paper 79-161, presented at AAS Conference, June 1979.

[6]Seltzer, S.M., "Special Issue on Dynamics and Control of Large Space Structures," *Journal of the Astronautical Sciences,* Vol. 27, No. 2, April-June 1979.

[7]Meirovitch, L., ed., *Proceedings of the Third VPI & SU/AIAA Symposium on Dynamics and Control of Large Flexible Spacecraft,* Blacksburg, Va., June 1981.

[8]"ACOSS Five (Active Control of Space Structures)," Phase 1A Final Report prepared by Lockheed Missiles & Space Co., Inc., Sunnyvale, Calif., for DARPA under Contract F30602-80-C-0101, Sept. 1981.

[9]Martin, G.D. and Bryson, A.E., "Attitude Control of a Flexible Spacecraft," *Journal of Guidance and Control,* Vol. 3, Jan.-Feb. 1980, pp. 37-41.

[10]Wie, B. and Bryson, A.E., "Attitude Control of a Triangular Truss in Space," Paper 77-2, presented at IFAC 8th World Congress, Kyoto, Japan, Aug. 1981.

[11]Rosenthal, D.E. and Cannon, R.H., "Experiments with Noncolocated Control of Flexible Structures," AIAA Paper 81-1841, Aug. 1981.

[12]Wie, B., Lehner, J.A., and Plescia, C.T., "Roll/Yaw Control of Flexible Spacecraft Using Skewed Bias Momentum Wheels," AIAA Paper No. 84-1962, Aug. 1984.

[13]Abdel-Rahman, T.M., "The Effects of Structural Flexibility on the Nonlinear Attitude Control of Spacecraft," Univ. of Toronto, Toronto, Canada, UTIAS Rept. 222, Dec. 1977.

[14]Bittner, H., Fischer, H.D., and Surauer, M., "Design of Reaction Jet Attitude Control Systems for Flexible Spacecraft," IFAC Conference, Automatic Control in Space, The Netherlands, 1982.

[15]Millar, R.A. and Vigneron, F.R., "Attitude Stability of a Pseudorate Jet-Controlled Flexible Sapcecraft," *Journal of Guidance and Control,* Vol. 2, March-April 1979, pp. 111-118.

[16]Bonello, D.P. and Basuthakur, S., "A Kalman Filter Thruster Controller for Precision Three Axis Spacecraft Attitude Control During Velocity Adjust Maneuvefrs," *Proceedings of the AIAA Guidance and Control Conference,* Palo Alto, Calif.

[17]Chan, F.N., Ford Aerospace and Communications Corporation Patent Application for: Method and Apparatus for Thruster Transient Control, US(SN)487-364 filed April 21, 1983.

[18]Likins, P.W. and Fleischer, G.E., "Results of Flexible Spacecraft Attitude Control Studies Utilizing Hybrid Coordinates," *Journal of Spacecraft and Rockets,* Vol. 8, March 1971, pp. 264-273.

[19]DeBra, D.B., "Pulse Modulators," Dept. of Aero/Astro, Stanford Un veristy, Stanford, Calif., AA 277 Class Note, 1980.

[20]Chan, F.N., Ford Aerospace and Communications Corporation Patent Application for: Digital PWPF Three-Axis Spacecraft Attitude Control US(SN)407-196 filed Aug. 11, 1982.

[21]Franklin, G.F. and Powell, J.D., *Digital Control of Dynamic Systems,* Addison-Wesley Pub. Co., Reading, Mass., 1980.

[22]Bryson, A.E., "Some Connections between Modern and Classical Control Concepts," *Journal of Dynamic Systems, Measurements and Control,* Vol. 101, Sept. 1979, pp. 92-98.